RESEARCH ARTICLE

Case studies of the wind field around Ny-Ålesund, Svalbard, using unmanned aircraft

Martin Schön,[1] Irene Suomi,[2] Barbara Altstädter,[3] Bram van Kesteren,[1] Kjell zum Berge,[1] Andreas Platis,[1] Birgit Wehner,[4] Astrid Lampert[3] & Jens Bange[1]

[1]Department of Geosciences, Tübingen University, Germany
[2]Finnish Meteorological Institute, Helsinki, Finland
[3]Technische Universität Braunschweig, Braunschweig, Germany
[4]Leibniz Institute for Tropospheric Research, Leipzig, Germany

Abstract

The wind field in Arctic fjords is strongly influenced by glaciers, local orography and the interaction between sea and land. Ny-Ålesund, an important location for atmospheric research in the Arctic, is located in Kongsfjorden, a fjord with a complex local wind field that influences measurements in Ny-Ålesund. Using wind measurements from UAS (unmanned aircraft systems), ground measurements, radiosonde and reanalysis data, characteristic processes that determine the wind field around Ny-Ålesund are identified and analysed. UAS measurements and ground measurements show, as did previous studies, a south-east flow along Kongsfjorden, dominating the wind conditions in Ny-Ålesund. The wind measured by the UAS in a valley 1 km west of Ny-Ålesund differs from the wind measured at the ground in Ny-Ålesund. In this valley, we identify a small-scale catabatic flow from the south to south-west as the cause for this difference. Case studies show a backing (counterclockwise rotation with increasing altitude) of the wind direction close to the ground. A katabatic flow is measured near the ground, with a horizontal wind speed up to 5 m s^{-1}. Both the larger-scale south-east flow along the fjord and the local katabatic flows lead to a highly variable wind field, so ground measurements and weather models alone give an incomplete picture. The comparison of UAS measurements, ground measurements and weather conditions analysis using a synoptic model is used to show that the effects measured in the case studies play a role in the Ny-Ålesund wind field in spring.

Keywords

Microscale meteorology; boundary layer; wind measurement; aircraft measurement; Kongsfjorden; Arctic fjord

Correspondence

Martin Schön, Department of Geosciences, Tübingen University, Schnarrenbergstraße 96, DE-72076 Tübingen, Germany.
Email: martin.schoen@uni-tuebingen.de

Abbreviations

ABL: atmospheric boundary layer
ALADINA: Application of Light-weight Aircraft for Detecting in situ Aerosols
AROME Arctic: Application of Research to Operations at Mesoscale (numerical weather prediction model, provided by the Norwegian Meteorological Institute)
ARTIST: Arctic Radiation and Turbulence Interaction Study (joint Finnish, German and Italian field measurement campaign with ground and airborne measurements, conducted in 1998 in Svalbard)
AWIPEV: Alfred Wegener Institute for Polar and Marine Research and Polar Institute Paul Emile Victor (joint German–French Arctic research station in Ny-Ålesund, Svalbard)
IMU: inertial measurement unit (GPS and movement sensors are combined to determine the position and movement vector of the vehicle carrying the IMU)
MASC: Multiple Purpose Airborne Sensor Carrier (electrically powered UAS with a wingspan of 4 m equipped with sensors to measure the wind vector, temperature and humidity in the ABL)
NILU: Norwegian Institute for Air Research
NWP: numerical weather prediction
SODAR: sonic detection and ranging (instrument for wind profiling)
UAS: unmanned aircraft system (includes aircraft capable of automatic flight, the controller on the ground and the sensor payload mounted on the aircraft)

Introduction

When researching the Arctic atmosphere to assess the impact of climate change, data from measurement stations play a significant role. For this reason, several internationally operated research stations in the Arctic provide long-term measurements. Located in Kongsfjorden, a fjord in northwest Spitsbergen, an island in the Svalbard archipelago (latitude: 78.923, longitude: 11.909; Figs. 1, 2), the village of Ny-Ålesund hosts 16 permanent stations from 10 different

Citation: *Polar Research* 2022, *41*, 7884, http://dx.doi.org/10.33265/polar.v41.7884

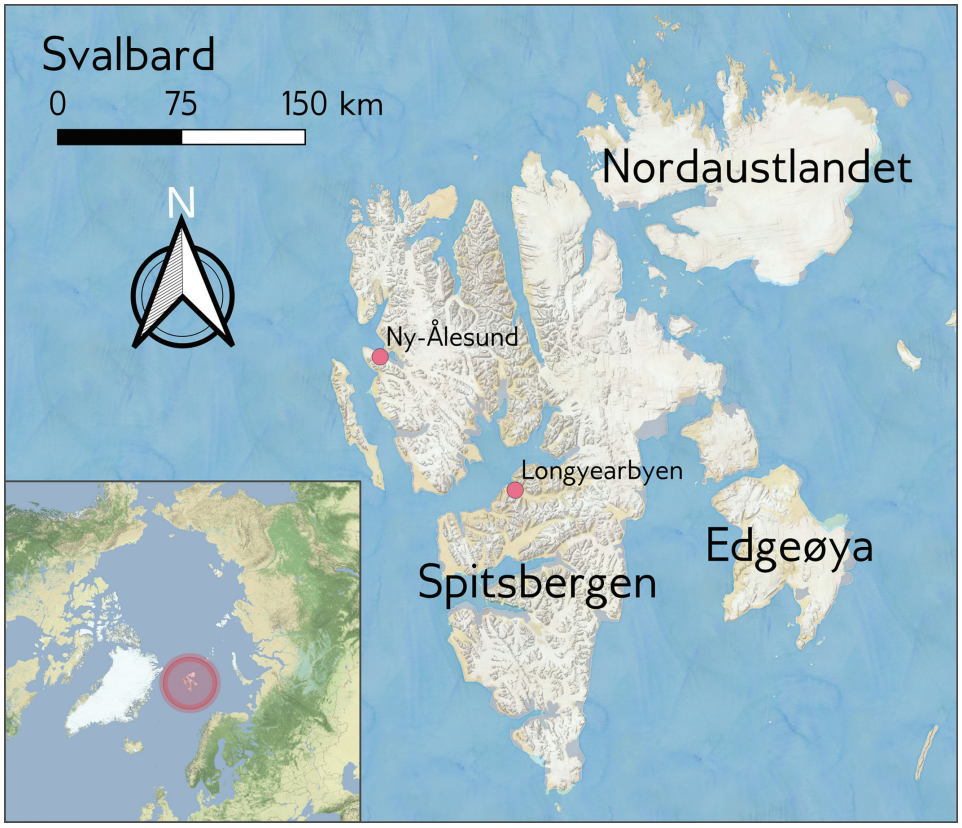

Fig. 1 Location of this survey, in Ny-Ålesund, on the island of Spitsbergen in the Svalbard archipelago. (Main map: Topo Svalbard, https://toposvalbard.npolar.no/, Norwegian Polar Institute. Inset map: Tiles by Stamen Design, under CC BY 3.0. Data by OpenStreetMap, under ODbL.)

countries. These research stations conduct meteorological, aerosol and trace gas measurements. Since local wind fields in Arctic fjords such as Kongsfjorden can deviate significantly from synoptic conditions (Svendsen et al. 2002), an understanding of this local wind field is crucial for the correct interpretation of the atmospheric measurements in Ny-Ålesund. For example, tethersonde measurements by Ferrero et al. (2016) show the importance of ABL properties like ground-based inversions and shear layers in the vertical wind profile for understanding the transport of aerosol particles. Aerosol particle measurements with the UAS ALADINA by the Technische Universität Braunschweig (Altstädter et al. 2015; Lampert et al. 2020; Petäjä et al. 2020) show the high vertical variability of aerosol concentration in the ABL and the need for understanding the local wind field influencing the transport processes.

The wind field in Arctic fjords such as Kongsfjorden is subjected to forcings by a highly variable terrain and significant thermal differences between open or frozen water and exposed soil or glacier ice. At larger scales, temperature differences between fjord water and open sea and synoptic processes play a role. Temperature and moisture inversions are common in the Arctic ABL (Egerer et al. 2021). Thermal differences between frozen and open water can lead to shallow convection and the development of internal boundary layers (Svendsen et al. 2002). Characteristic phenomena are low-level jets, which regularly occur because of katabatic flows (Vihma et al. 2011). Meltwater from the glaciers surrounding an Arctic fjord influences its water temperature. Cold, dense air flows from glaciers to the mouth of the fjord (Svendsen et al. 2002). In Kongsfjorden, these drainage flows often lead to higher wind speeds within the Arctic ABL, which typically has a depth of 250 m, and inverse wind directions compared to the synoptic conditions (Beine et al. 2001; Argentini et al. 2003).

For Arctic fjords, numerical models cannot reproduce these complex interactions reliably (Tjernström & Graversen 2009), while ground measurements and vertical profiles from radiosondes do not give enough information on the horizontal variability of the local wind field to determine its structure.

In 1998, the ARTIST project carried out a campaign to investigate SODAR profiles combined with the ground-based in situ measurements at Ny-Ålesund and the mountain Zeppelinfjellet (474 m a.s.l.,

Citation: *Polar Research* 2022, *41*, 7884, http://dx.doi.org/10.33265/polar.v41.7884

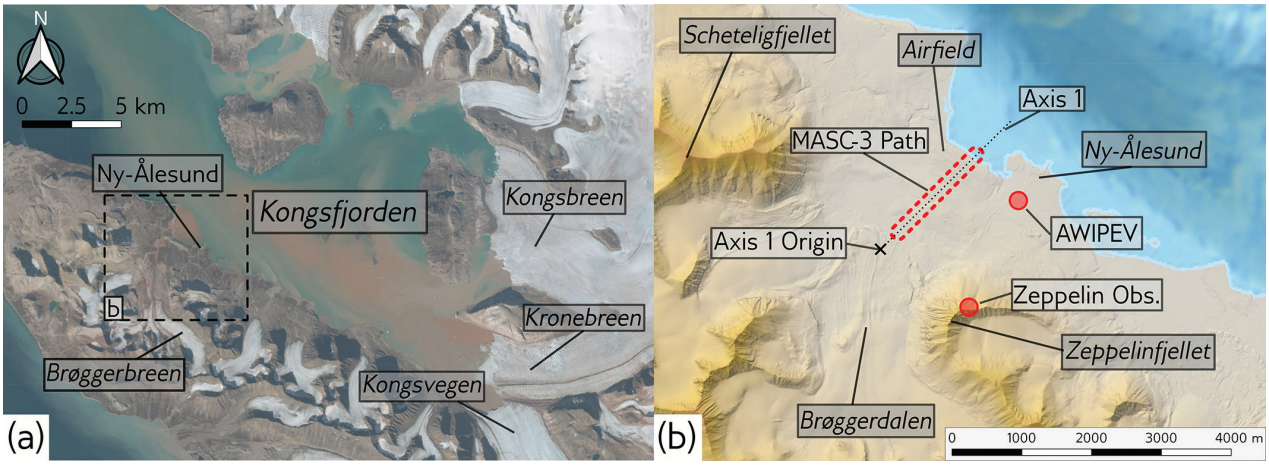

Fig. 2 (a) Overview map of the fjord Kongsfjorden. The glaciers Kongsbreen, Kronebreen and Kongsvegen are in the east and south-east. The sea is to the west. The smaller Brøggerbreen glacier originates south-west of Ny-Ålesund. The rectangle in (a) shows the extent of the zoomed-in map (b). (b) Detailed map of the area around Ny-Ålesund. West of Ny-Ålesund is the Brøggerdalen valley, with the Brøggerbreen glacier further up the valley, visible in (a). The highest mountains in the vicinity are Scheteligfjellet (719 m a.s.l.) and Zeppelinfjellet (556 m a.s.l.). The Zeppelin Observatory is located on Zeppelinfjellet, at 474 m a.s.l. Within the village of Ny-Ålesund is AWIPEV, which is the location of the continuous ground measurements and the radiosonde ascents presented in Fig. 4. The flight pattern of MASC-3 (red dashed line) followed along axis 1 (black dashed line), reaching into the Brøggerdalen in the south-west and passing over the Ny-Ålesund Airfield in the north-east. (Maps by Topo Svalbard, https://toposvalbard.npolar.no/, Norwegian Polar Institute/USGS Landsat.)

approximately 2 km south-west of Ny-Ålesund; Fig. 2). The results show that the two prevailing wind directions in the ABL are oriented along the fjord: In spring, the air flows from the Kongsbreen and Kongsvegen glaciers in the south-east to the mouth of the fjord in the north-west (Hartmann et al. 1999; Argentini et al. 2003). During summer, the primary wind direction reverses (Beine et al. 2001). This seasonal pattern of down-fjord flows in winter and up-fjord flows in summer is typical for large fjords (Svendsen et al. 2002). In Ny-Ålesund, this flow along the fjord with an east–south-east or south-east wind direction is dominant during spring. Local katabatic flows from the Zeppelinfjellet slope cause a secondary, less frequent, south–south-west to south-west wind direction and may also cause differences in wind direction between AWIPEV and Zeppelinfjellet (Beine et al. 2001).

To validate these findings and to investigate the horizontal variability of the wind field around Ny-Ålesund, the UAS MASC-3 is used in conjunction with ground-based measurements and radiosondes. During a measurement flight, MASC-3 can close the gap between separate ground measurement locations while also creating a vertical profile of the ABL, essentially creating a two-dimensional snapshot of the ABL conditions during a measurement flight. An in situ measurement system like MASC-3 can collect data even under conditions difficult for remote sensing systems (e.g., low aerosol concentrations).

During April and May 2018, the MASC-3 research UAS operated by the University of Tübingen performed in situ measurements west of Ny-Ålesund. The measurements took place along Brøggerdalen, a valley about 2 km wide, west of Ny-Ålesund. The glacier Brøggerbreen lies in the south-western part of the valley (Fig. 2). We compare 10 measurement flights presented here with simultaneous wind measurements on the ground. Two flights from 1 May 2018 are described as case studies, identifying a local, small-scale katabatic flow as an important factor in the local wind field. In the end, we present a high-resolution map of the local wind field around Ny-Ålesund.

Methods

Site description

The ground measurements of wind and temperature in this study come from two sources: the Norwegian observatory on the mountain Zeppelinfjellet, south-west of Ny-Ålesund, and, in Ny-Ålesund, the observatory of the French–German research base AWIPEV (Fig. 2). Ny-Ålesund is situated in Kongsfjorden, which is up to 11 km wide and 30 km long. The fjord opens up to the sea in the north-west. In the south-east, the glaciers Kongsbreen and Kongsvegen join the fjord. Steep mountains reaching up to 700 m in height surround the fjord. Ny-Ålesund itself is located on the south-west coast of the fjord. South of the village, Zeppelinfjellet rises to a height

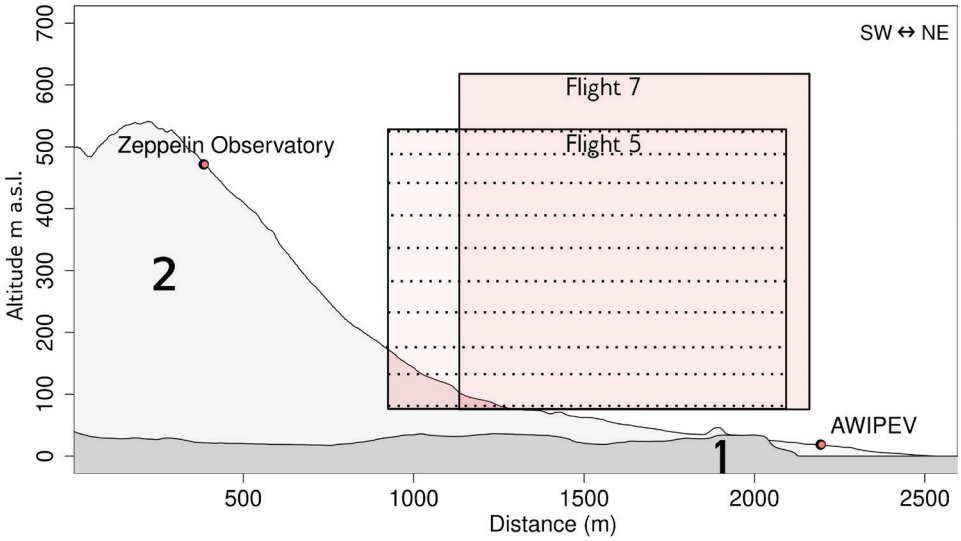

Fig. 3 Cross-section showing the terrain along the Brøggerdalen beneath the MASC-3 flight path (Fig. 2) and Zeppelinfjellet (light grey), the location of AWIPEV and Zeppelin Observatory and the vertical and horizontal extent of the two MASC-3 flights on 1 May 2018 (red squares). To illustrate the measurement pattern, the flight path of MASC-3 during flight 5 is included as a dashed line. The vertical axis shows the altitude in m a.s.l. The horizontal axis is the distance in m along the flight path originating at a reference point (marked in Fig. 2). Elevation data for cross-section from Arctic DEM (Porter 2018).

of 557 m a.s.l. The Zeppelin Observatory is situated below the summit, on the north-western edge of a ridge, at 474 m a.s.l. The airfield of Ny-Ålesund is north-west of the village, where Brøggerdalen opens up into the fjord. The cross-section in Fig. 3 shows the horizontal and vertical extent of the two case studies presented here. During the measurement period, the fjord was ice-free. The ground around Ny-Ålesund was completely covered with snow until mid-May.

MASC-3 sensor system

The UAS MASC-3 is an electrically powered aircraft with a wingspan of 4 m and a take-off weight between 5 and 8 kg, depending on battery weight. A Pixhawk 2.1 Cube Autopilot running the Arduplane firmware controls automatic flight and enables MASC-3 to follow a predefined set of waypoints during a measurement flight (Rautenberg et al. 2019). The measurement flights presented in this work lasted between 1 and 1.5 hours at a constant true airspeed of 18.5 m s^{-1}. All flights were conducted within the line of sight around the Ny-Ålesund airfield. MASC-3 carries a meteorological sensor package developed by the Environmental Physics Group of the University of Tübingen. The set-up is based on the Meteorological Mini-Aerial Vehicle 2 and MASC-2 aircraft (van den Kroonenberg et al. 2008; Wildmann, Hofsäß et al. 2014). For wind, temperature and position measurements, MASC-3 uses a five-hole probe, a fine wire platinum resistance thermometer (Wildmann et al. 2013) and an IMU with a GPS receiver. In order to measure the three-dimensional wind vector and air temperature with a resolution of up to 30 Hz, MASC-3 samples data with a frequency of 100 Hz (Wildmann, Ravi et al. 2014). Rautenberg et al. (2019) provide a detailed description of the complete MASC-3 set-up. MASC-3 can fly in wind speeds up to 15 m s^{-1}; to ensure safe take-off and landing the maximum surface wind speed should not exceed 10 m s^{-1}. In the configuration flown in Ny-Ålesund, MASC-3 can only be used in line of sight, excluding flying in fog or clouds. MASC-3 cannot be flown in heavy rain.

Measurement flights

A total of 18 measurement flights were performed between 24 April and 25 May 2018 (data set: Schön et al. 2022). The first 10 flights between 24 April and 12 May 2018, which are presented here, follow the flight pattern depicted in Figs. 2b and 3. The date, time frame, minimum measurement altitude (h_{min} [m a.s.l.]) and maximum measurement altitude (h_{max} [m a.s.l.]) of each flight are listed in Table 1. The flights are referred to hereafter by their flight number. The minimum and maximum flight altitudes for each flight vary with weather conditions, visibility and coordination with Air Traffic.

During a measurement flight, MASC-3 starts at the lowest measuring altitude, repeating each measurement altitude in the pattern shown in Fig. 3 two times, maintaining a straight and level flight path and a constant true

Citation: *Polar Research* 2022, *41*, 7884, http://dx.doi.org/10.33265/polar.v41.7884

Table 1 Overview of the Multiple Purpose Airborne Sensor Carrier (MASC) measurement flights performed between 24 April and 12 May 2018. The two case studies on 1 May are highlighted in boldface.

Flight no.	Date	Time (UTC)[a]	h^{b}_{min} (m a.s.l)	h^{c}_{max} (m a.s.l.)	Altitudes of the measurement legs (m a.s.l.)[d]
1	2018-04-24	19:59–20:54	77	327	80, 100, 130, 150, 180, 200, 230, 280, 320
2	2018-04-26	12:51–13:58	73	466	70, 90, 110, 130, 160, 180, 220, 270, 320, 370, 410, 460
3	2018-04-29	19:28–20:51	72	331	70, 90, 110, 140, 160, 180, 210, 230, 280, 330
4	2018-04-29	21:51–23:12	75	326	80, 90, 110, 140, 160, 180, 180, 210, 230, 280, 330
5	**2018-05-01**	**09:31–10:39**	**77**	**528**	**80, 90, 140, 190, 240, 280, 330, 380, 430, 480, 530**
6	2018-05-01	11:47–13:08	64	519	60, 80, 130, 180, 230, 270, 320, 370, 420, 470, 520
7	**2018-05-01**	**15:30–16:55**	**66**	**619**	**70, 80, 130, 180, 230, 330, 420, 520, 620**
8	2018-05-07	11:10–11:56	84	422	80, 110, 130, 160, 180, 230, 330, 420
9	2018-05-12	14:38–15:59	64	410	70, 130, 180, 220, 270, 320, 360, 410
10	2018-05-12	17:25–18:46	75	540	80, 90, 140, 240, 340, 440, 540, 640

[a]The timeframe of the measurement. [b]The lowest measurement altitude. [c]The maximum measurement altitude. [d]Rounded to the nearest 10 m.

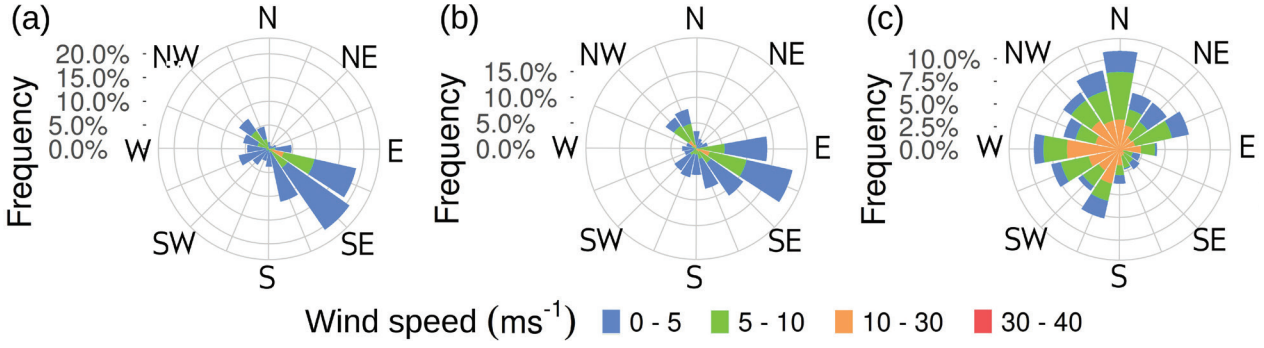

Fig. 4 Wind roses for April and May of 2017 to 2020: (a) ground data from the AWIPEV observatory (Maturilli 2020a, b); (b) radiosonde data (Maturilli 2020c) from 400 to 500 m a.s.l., corresponding to the altitudes around Zeppelin Observatory (450 m a.s.l.); and (c) 2000–2100 m a.s.l., above the highest terrain in Svalbard. Radiosonde data are from the daily launches at AWIPEV (11:00 UTC), at 1 Hz resolution. Ground station data are from a cup anemometer/wind vane combination at AWIPEV (10 m above ground, 21 m a.s.l.), provided as 1-min average. The dominant wind direction in the AWIPEV measurements at sea level is east–south-east to south-east, which corresponds to a flow along the fjord.

airspeed of 18.5 m s^{-1}. Accordingly, each of these repetitions consists of two straight and level sections, referred to as legs. The respective altitudes of the measurement legs for each flight are listed in Table 1. The vertical distance between measurement legs is typically 20–30 m below 200 m a.s.l. and 40–50 m above. This increases the vertical resolution close to the ground, where a high vertical variability in wind and temperature is expected.

After completing all repetitions at one altitude, MASC-3 proceeds to the next altitude. This is repeated up to the maximum measurement altitude. Whenever possible, the maximum altitude was higher than the Zeppelin Observatory (474 m a.s.l.) to fully cover the vertical variability of the wind field between the surface and the observatory.

In Fig. 2b, the flight pattern is shown as a dashed red line on a map of the area around Ny-Ålesund. Figure 3 shows the same flight pattern as a cross-section, exemplified for the extents of flights 5 and 7. In the cross-section of flight 5, dashed lines indicate the path of the measurement legs.

Ground-based, NWP and radiosonde data

Ground-based measurements, radiosonde data and NWP model data are compared with MASC-3 data. Observations are obtained from AWIPEV ground-based and radiosonde measurements for April and May from 2017 to 2020 (Maturilli 2020a, b, c). At the AWIPEV observatory, wind measurements are taken at 10 m above the surface level (22 m a.s.l.) using a cup anemometer and wind vane combination, provided as 1-min averages. The radiosonde data used in Fig. 4 are from the daily radiosonde launches (Vaisala RS41) in Ny-Ålesund. The radiosonde

is launched every day at 11:00 UTC. The position of the radiosonde is determined by GPS data, which is used to calculate wind speed and wind direction.

Data from the Zeppelin Observatory are provided by NILU, measured at 474 m a.s.l. (Aas 2007a, b). At this observatory, a cup anemometer is used for wind speed, a wind vane for wind direction and a platinum resistance thermometer for temperature measurements, provided as 1-hour average. For the case studies, synoptic conditions during the flights in Table 1 were analysed based on operational AROME Arctic NWP model cycle, version 40h1.1, with output provided by the Norwegian Meteorological Institute (MET Norway 2021). The model system provides regional short-range forecasts for the European Arctic with 2.5 km horizontal resolution and 65 vertical levels (Müller et al. 2017; Køltzow et al. 2019). The results presented in this study are based on forecasts initiated at 00:00 UTC on each flight day.

Data processing

MASC-3 produces a high-resolution time series of the wind vector and temperature for each measurement leg. This results in multiple time series per measured altitude. The resolution of those measurements is sufficient to resolve smaller turbulent eddies even in the submetre range (Rautenberg et al. 2019). However, to determine the wind field, it is not individual eddies that have to be considered, but the average wind direction, wind speed and temperature. Therefore, a time average must be taken that is long enough to encompass the largest relevant eddies. To accomplish this, the averaging time must be larger than the integral time scale of each component of the three-dimensional wind vector (Garratt 1992). For the case studies presented here, the integral time scales of u, v and w were calculated for each leg and, in all cases, were found to be less than 9 s. A moving average of 9 s was, therefore, applied for the cross-section plots (Fig. 5). For the vertical profiles (Fig. 6), all measurement legs at each measurement altitude were averaged.

MASC-3 data for the case studies are visualized with two different methods. Two-dimensional cross-sections are used to visualize the vertical and horizontal variability of the wind field and temperature (Fig. 5). The position of the cross-section and the horizontal and vertical extent of the measurement flights are illustrated in Figs. 2b and 3. The second plotting method for the two case studies is vertical profiles (Fig. 6). They are used to compare MASC-3 data with the ground measurements at AWIPEV and the Zeppelin Observatory to investigate the relationship between the wind conditions at AWIPEV and the Observatory. Each point in the vertical profile represents the average of all measurement legs at the respective altitude. At the corresponding altitude, measurement data from AWIPEV and the Zeppelin Observatory for the measurement flight duration are included in the profiles. A MASC-3 temperature measurement from the ground is included to provide a complete vertical profile of temperature.

Results

Long-term observations of the wind field

The wind roses of the long-term wind conditions for April and May between 2017 and 2020 show that the dominant wind direction at ground level in Ny-Ålesund was east–south-east or south-east, i.e., along the shoreline of Kongsfjorden (Fig. 4a). This wind direction corresponds to the flow along the fjord described in literature (Beine et al. 2001; Svendsen et al. 2002; Argentini et al. 2003; Esau & Repina 2012). Two secondary wind directions are visible: west–north-west, corresponding to an up-fjord flow, which is more prevalent during summer (Svendsen et al. 2002), and a west–south-west to south-west wind direction. Between 400 and 500 m a.s.l. (corresponding to the altitude of the Zeppelin Observatory at 474 m a.s.l.), the radiosonde data show a dominant east–south-east to south-east wind direction (Fig. 4b), which corresponds to the ground measurement. The second most common wind directions were the north–north-west and north-west, with additional peaks in the wind rose at the south–south-west and south–south-east. At 2000–2100 m a.s.l., above the highest mountains of Svalbard (1713 m a.s.l.), the wind rose of the radiosonde measurements (Fig. 4a) shows a dominant north wind direction, together with a broader range of wind directions from the south–south-west to north–north-west.

MASC-3 measurement flights 24 April—12 May 2018

Ten measurement flights were performed between 24 April and 12 May 2018, using the flight pattern shown in Fig. 2b. To provide an overview of the measurement data, Table 2 shows the mean wind direction and horizontal wind speed during the measurement flights at AWIPEV and the Zeppelin Observatory. For MASC-3 flight data, this information is displayed for the lowest altitude h_{min} and highest altitude h_{max} (see Table 1 for the altitudes). The dominant south-east to east–south-east flow along the fjord seen in the wind roses (Fig. 4) was measured at AWIPEV during flights 3–8, when the prevailing wind direction at the Zeppelin Observatory was south. The

Citation: *Polar Research* 2022, *41*, 7884, http://dx.doi.org/10.33265/polar.v41.7884

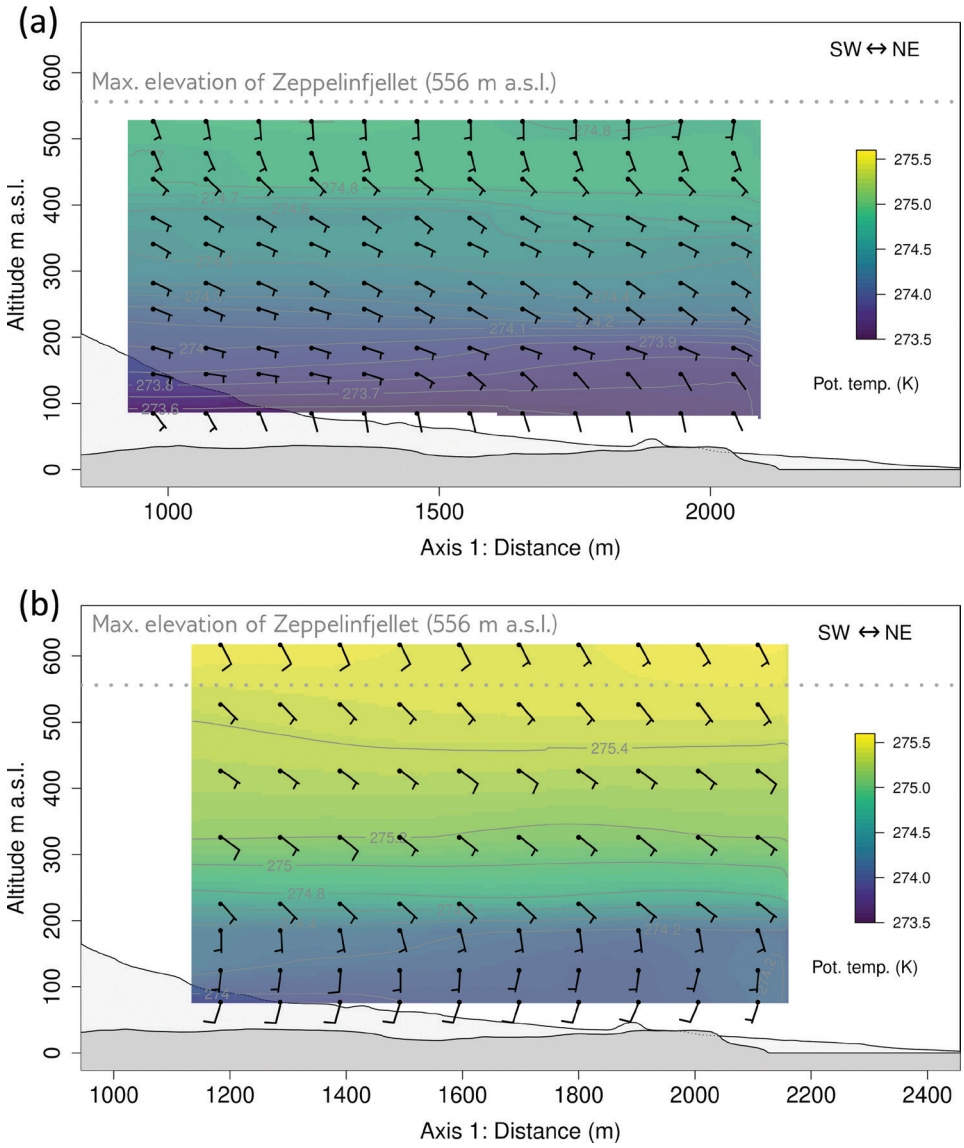

Fig. 5 Cross-sections of MASC-3 measurements: (a) flight 5 on 1 May 2018, 09:31–10:39 UTC and (b) flight 7 from 15:30 to 16:55 UTC. In the cross-sections, black wind barbs show the horizontal wind speed and wind direction measured by MASC-3 for every measurement altitude. Dashes at the end of the barb represent horizontal wind speed. Barbs without bars represent wind speed between 0 and 2 knots, a short bar 5 ± 2 knots and a long bar 10 ± 2 knots. Potential temperature is displayed along a colour ramp. The temperature values in the altitudes between measurements are linearly interpolated. The dark grey silhouette shows the terrain directly below the measurement (axis 1). The light grey silhouette shows the maximal terrain elevation in the vicinity of the measurement (axis 2). The vertical axis shows the altitude in m a.s.l. The horizontal axis is the distance in m along axis 1, originating at a reference point (marked in Fig. 2).

mean wind speed at AWIPEV ranges 0.7–2.9 m s^{-1}, while Zeppelin showed slightly higher wind speed, 1–3 m s^{-1}. Since this south-east to east–south-east wind direction was the main wind direction in the long-term observations at AWIPEV for April and May, the interpretation of the MASC-3 measurements will focus on flights 3–8.

Comparing the AWIPEV measurements with the MASC-3 measurements at the lowest measurement altitude shows that, in most cases, MASC-3 measured similar wind speeds as the AWIPEV observatory (in the range of ±1 m s^{-1}). For flights 7 and 10, MASC-3 measured a higher wind speed than at the AWIPEV. Generally, the wind speed during all 10 flights was low, between 0.5 and 4.5 m s^{-1}.

The dominant wind direction at AWIPEV was south to east–south-east (flights 1–7). The corresponding wind

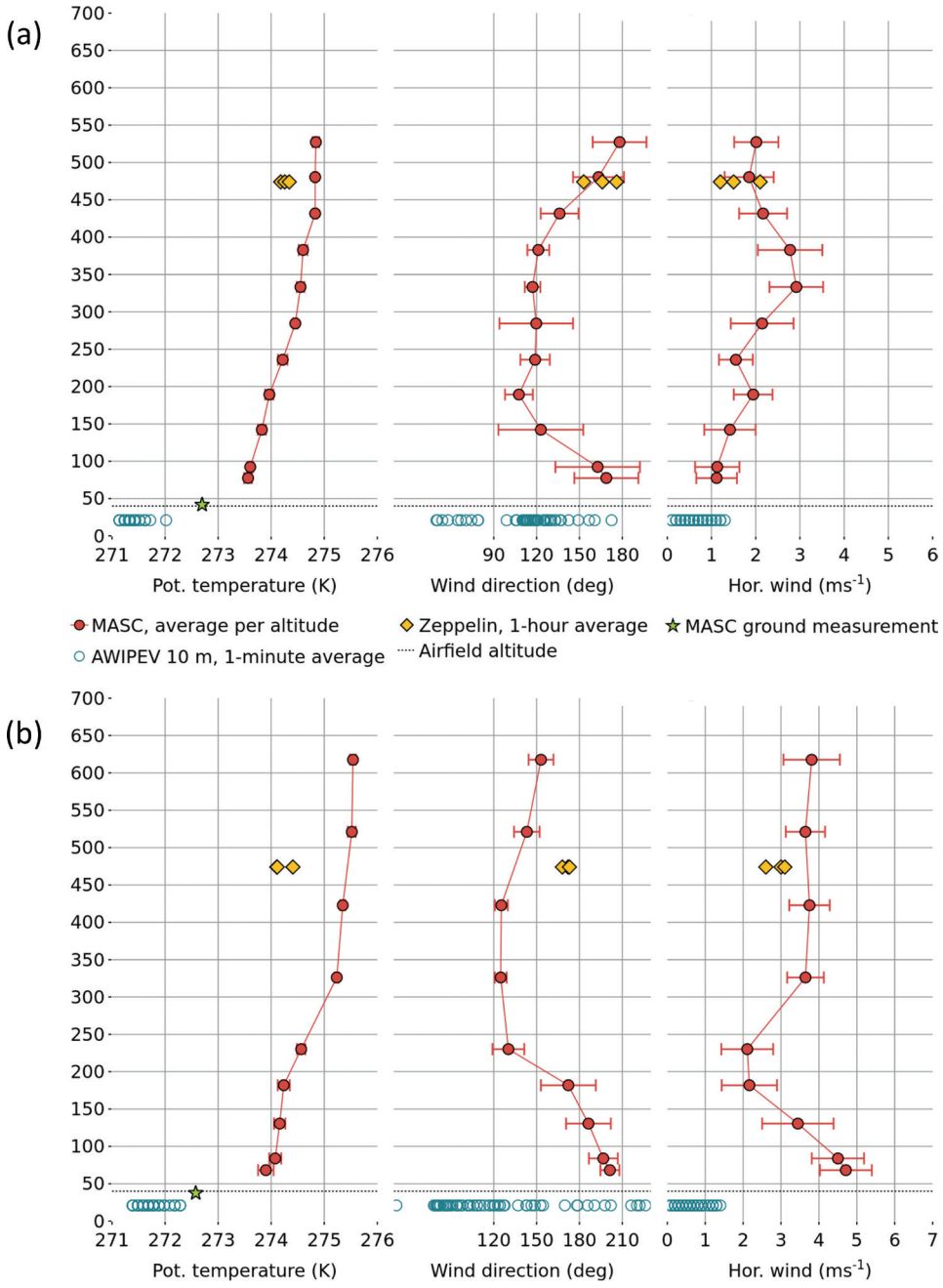

Fig. 6 Vertical profiles of potential temperature, wind direction and horizontal wind speed for MASC-3 measurements and ground-based measurements at AWIPEV and the Zeppelin Observatory: (a) flight 5, 1 May 2018 09:31–10:39 UTC and (b) flight 7, 15:30–16:55 UTC. For MASC-3, the horizontal bars show the standard deviation within measurement altitude. AWIPEV data are provided as 1-min average, and Zeppelin data as 1-hour average.

direction at MASC-3 was either south-east (flights 3, 4 and 6) or more south to west than at AWIPEV (flights 1, 2, 5 and 7). The last three flights (flights 8, 9 and 10) were exceptions to this pattern, and for flights 9 and 10, different wind conditions prevailed at AWIPEV, with west–north-west and south-west wind, respectively. A recurring pattern in the vertical profiles measured by MASC-3 near Ny-Ålesund was a backing (counterclockwise rotation with increasing altitude) of the wind direction from the lowest altitude up to 120 m – 230 m a.s.l. For example, during flight 5, the wind direction rotated from the south at 77 m a.s.l. to an east–south-east wind direction at 180 m a.s.l. by 80°. Since this backing is a typical feature of the wind profiles measured with

Citation: *Polar Research* 2022, *41*, 7884, http://dx.doi.org/10.33265/polar.v41.7884

MASC-3, it is categorized using the two values in the wind direction profile column of Table 2, b_{top} and $b°$.

Case study selection: 1 May 2018

For a detailed look at the wind field characteristics from flight data, two measurement flights are selected as case studies. Flight 5, which took place on 1 May 2018 between 09:31 and 10:39 UTC, at altitudes ranging 77–528 m a.s.l., showed the backing of the wind direction described above, as well as the typical south-west wind direction at AWIPEV. Furthermore, data are available for this flight up to 528 m altitude, i.e., the vertical profile of the wind was measured up to the altitude of the Zeppelin Observatory. The vertical profile of flight 5 is typical for the available vertical profiles. It also contains data above 474 m a.s.l., so a comparison with the Zeppelin Observatory is possible. The second case study, flight 7, also took place on 1 May 2018, 15:30 to 16:55 UTC, at altitudes between 66 and 619 m a.s.l. This flight also showed the backing in the wind direction. In addition, in this flight, the wind speed shows a strong local maximum at the lowest flight altitude, along with a south–south-west wind direction (Figs. 5, 6, and Table 2). This local maximum in wind speed at the lower flight altitudes was not a common feature and was only measured in flights 2, 7 and 8. In the profile cross-section (Fig. 2b), the case studies' extent on 1 May is shown.

To put the case studies into context, long-term observations from radiosondes and ground stations are used to describe the typical wind speed and wind directions for April and May in Ny-Ålesund. Then, the synoptic situation for 1 May 2018 is described. Finally, the case studies are described in detail, with cross-sections and vertical profiles, as explained in the data processing section. The wind field's vertical variation for both flights on 1 May 2018 is shown using vertical profiles for potential temperature, wind direction and horizontal wind speed (Fig. 6). The profiles show the averaged values and the standard deviation in the high-resolution data for each measurement altitude for each flight.

The potential temperature measured at 10 m above the ground at AWIPEV was 2–2.5 K lower than at the lowest MASC-3 altitude during both flights. A possible reason for this is a surface-based temperature inversion. This is supported by a MASC-3 measurement on the ground directly after landing (Fig. 6). On the ground, MASC-3 measured 272.7 K for flight 5 and 272.6 K for flight 7. For flight 5, the potential temperature profile above the surface-based inversion measured with MASC-3 showed a weakly stable ABL from 273.6 K at 80 m to 274.9 K at 430 m a.s.l. and a neutral stratification between 430 m and 520 m a.s.l. For flight 7, there was still a weakly stable stratification at altitudes below 530 m a.s.l., but between 230 m and 320 m a.s.l., there was an inversion in the temperature profile, where the potential temperature increased by 0.8 K within a vertical distance of 90 m.

For flight 5, the wind direction at the lowest MASC-3 altitude was south. Above this altitude, there was backing in the wind direction to the east–south-east at 200 m a.s.l. This wind direction of east–south-east (to south-east), along Kongsfjorden, was also dominant in the long-term measurements in Ny-Ålesund (Fig. 4). Above 200 m a.s.l., the wind direction rotated from the east–south-east to the south, at 530 m a.s.l. The wind speed increased with altitude, from 1 m s^{-1} at the lowest measurement altitude to a maximum wind speed of 2.9 m s^{-1} at 380 m a.s.l. While the measured horizontal wind speed and wind direction at Zeppelin lay largely within the standard deviation of the MASC-3 values for the same altitude, AWIPEV data showed a low wind speed below 1 m s^{-1}. The morning wind direction measurement at AWIPEV had a very high standard deviation due to the low wind speed.

For flight 7, from the lowest MASC-3 altitude of 60–230 m a.s.l., there was backing in the wind direction from the south–south-west to the south-east. Between 230 and 420 m a.s.l., the wind direction was the south-east. Above 420–620 m a.s.l., the wind direction rotated from the south-east to the south–south-east. The maximum wind speed was 4–5 m s^{-1} at 60 m a.s.l., decreasing with altitude to 2 m s^{-1} at 180 m a.s.l. and then increasing again to 3–4 m s^{-1} above 300 m a.s.l. Horizontally, the wind speed and wind direction above 230 m a.s.l. were homogeneous, with similar values over the valley and the shore (Fig. 5).

Synoptic conditions on 1 May 2018

Towards the end of April 2018, a large low-pressure system deepened east of Greenland. On its eastern side, a ridge of high pressure stretched from the northern coast of Scandinavia to the western coast of Svalbard. According to the AROME Arctic NWP model output, the central line of the ridge was located roughly along the western coast of Spitsbergen at 00:00 UTC on 1 May and moved gradually inland during the day (Fig. 7). The low wind speed at the 925 hPa level and above with a west–south-west direction in the morning of May changed to a south–south-west direction with increasing wind speed towards the evening. AROME Arctic forecasts showed a warm-air advection by about 1.5 degrees in the 6 hours between 10:00 and 16:00 UTC (i.e., between the flights) at heights between 200 m and 1000 m a.s.l. (Fig. 8). This led to an increased thermal stratification near the surface.

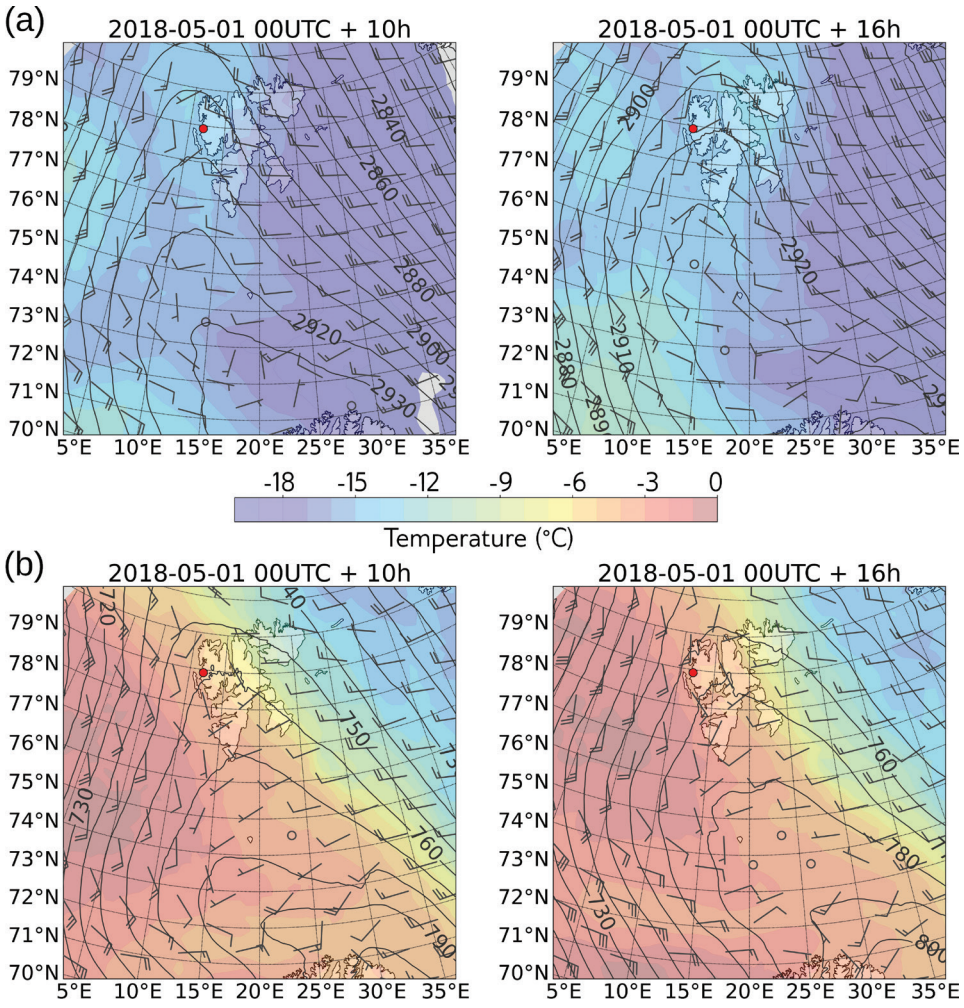

Fig. 7 Synoptic situation on 1 May 2018 based on operational forecasts of the AROME Arctic model (MET Norway 2021), (a) for the 700 hPa level and (b) for the 925 hPa level. Geopotential height (grey contours), temperature (colour contours) and wind barbs are shown. The output is shown for 10:00 UTC (left) and 16:00 UTC (right) on 1 May. The location of Ny-Ålesund is shown as a red dot.

Discussion

The measurements with MASC-3 are snapshots of the ABL, so it is useful to compare and contextualize them with long-term measurements. Cisek et al. (2017) analysed the multiannual monthly mean of wind speed from 2005 to 2016 in Ny-Ålesund, based on measurements by the AWIPEV station. For this timeframe, the maximum mean wind speed was between 5 and 6 m s^{-1} during November and December, with the minimum mean wind speed in August, at 2–3 m s^{-1}. The most common wind conditions at AWIPEV in April and May were east–south-east to south-east wind direction with low (less than 5 m s^{-1}) wind speeds, which is also supported by more recent AWIPEV data and radiosonde data (Fig. 4). Therefore, the measurements of MASC-3 (Table 2) were carried out under wind conditions typical for spring in Ny-Ålesund.

The typical wind direction measured at AWIPEV is east–south-east–south-east, which corresponds to the flow along the fjord. The wind direction measured by MASC-3 at lower altitudes, 80–200 m a.s.l., in Brøggerdalen, differs significantly from this flow along the fjord in both case studies on 1 May 2018 (Fig. 6). Only at higher altitudes, between 200 and 500 m a.s.l., MASC-3 did also measure this east–south-east–south-eastwind direction. MASC-3, therefore, showed a backing from the south–south-west at the lowest flight altitude to south-east at around 200 m a.s.l. In most of the MASC-3 flights (Table 2), this backing is exemplified by flight 5 (Fig. 6a), with a continuous, stable temperature profile and with a wind speed profile, in which the wind speed increased with altitude and had a maximum above 300 m a.s.l.

Flight 7 showed, in addition to the backing in the lower altitudes, other noteworthy features. The

Citation: *Polar Research* 2022, *41*, 7884, http://dx.doi.org/10.33265/polar.v41.7884

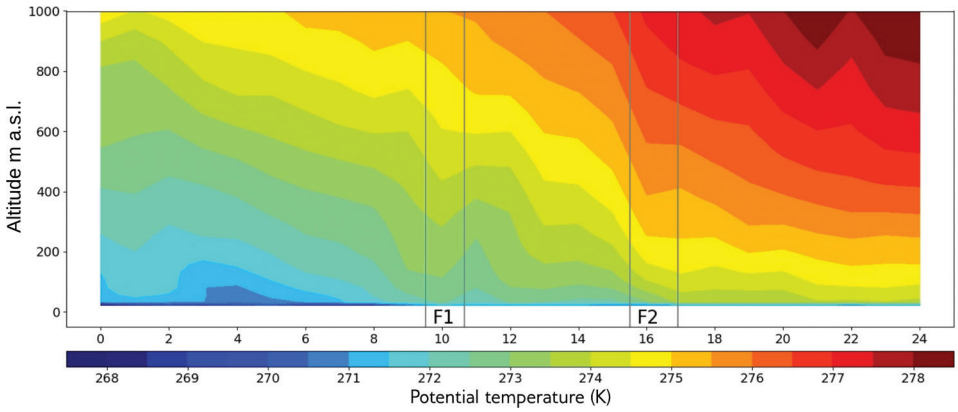

Fig. 8 Time-height cross-sections of potential temperature (Θ) at the grid point closest to Ny-Ålesund based on operational forecasts of AROME Arctic model starting from 00:00 UTC on 1 May 2018. F 5 and F 7 indicate the case study flight times by vertical lines showing the beginning and the end of each flight. Data are from the Norwegian Meteorological Institute (MET Norway 2021).

Table 2 Key measurement results for all flights listed in Table 1. For the period of the flights, the horizontal wind speed in m s^{-1} (v_h) and the wind direction (wd) in degrees are listed from the following sources: AWIPEV ground measurement at 10 m above ground, averaged MASC measurement values at lowest flight altitude (h_{min}, m a.s.l.), the mountain Zeppelinfjellet at 474 m a.s.l. and averaged MASC measurement values at maximum flight altitude (h_{max}, m a.s.l.). AROME Arctic (MET Norway 2021) wind speed (v_h) in m s^{-1} and wind direction (wd) for the 700 hPa and the 925 hPa pressure level provide information on the synoptic situation. AWIPEV data are averaged for the time interval of the measurement flight, and AROME and Zeppelin Observatory data are averaged for the time interval of the measurement flight rounded to the closest full hour. In addition, the structure of the backing of the wind direction with increasing altitude (backing, in degrees) is shown. For most of the measurement flights, there is a backing of the wind direction from the lowest altitude up to b_{top}, above that there is a veering of the wind direction. The amount of rotation of the wind direction between h_{min} and h_{max} is given in degrees with the value $b°$. The two case studies on 1 May are highlighted in boldface. See the results section for MASC-3 measurement flights from 24 April 2018 to 12 May 2018 for further explanation.

Flight no.	AWIPEV		MASC h_{min}		Zeppelin		MASC h_{max}		AROME 925 hPa		AROME 700 hPa		Backing	
	v_h	wd	v_h	wd	v_h	wd	v_h	wd	v_h	wd	v_h	wd	b_{top}	$b°$
1	1.7	SSE	1.6	SSW	1.5	SSE	3.9	SE	1.2	ENE	6.0	NNW	180	100
2	1.5	S	0.9	SSW	1	SW	1.8	NNE	2.1	W	6.5	NW	230	100
3	2.9	SE	1.9	SE	2.8	S	3	WSW	5.4	ESE	5.4	WSW	120	50
4	2	SE	3.1	SE	2.2	S	2	W	4.7	SSW	5.7	WSW	140	45
5	**0.7**	**SE**	**1**	**S**	**1.8**	**S**	**2**	**WSW**	**3.7**	**S**	**2.4**	**SW**	**180**	**80**
6	0.9	SE	1.7	SE	2.4	SSE	4	SW	5.0	SE	3.5	SSW		
7	**0.5**	**ESE**	**4.4**	**SSW**	**2.9**	**S**	**4**	**SW**	**6.3**	**SSE**	**6.4**	**SSW**	**200**	**80**
8	2.6	SE	3.5	ESE	3	S	4.5	WSW	8.8	S	9.7	SSW		
9	1.9	WNW	2.4	W	1.3	SE	2	WNW	7.8	WNW	11.3	NW	200	30
10	2	SW	3.8	SW	1.8	SSW	1.8	WNW	4.4	W	14.8	WNW		

maximum wind speed was at the lowest measurement altitude, with a decrease in wind speed up to 200 m a.s.l. (Fig. 6b). Also, the potential temperature profile was not as continuous as in flight 5: in flight 7, there was a sudden change in the temperature profile between 250 m and 300 m a.s.l. The change in the temperature profile and the higher wind speed coincided with the backing of the wind direction. These features are not visible in the AWIPEV data for the same timeframe, which shows very low wind speed below 1 m s^{-1} and the typical east–south-east to south-east wind direction.

The wind direction and wind speed deviation from the flow along the fjord were restricted to the lower, cold air layer in Brøggerdalen. This layer was continuous over the entire horizontal extent of the measurement flight, and its upper limit at approximately 200 m a.s.l. was related to the rotation of the wind direction from the south–south-west to the south-east (Fig. 5b). This cold air mass is, therefore, interpreted as katabatic flow, which moves near the ground towards the fjord, causing the south–south-west wind direction in the measurement area of MASC-3, but does not

influence the measurement at AWIPEV, which lies outside of the axis of Brøggerdalen (Fig. 9). The development of the katabatic flow is facilitated by the development of a more stable ABL during the day, which is visible in the AROME Arctic model (Fig. 8). Generally, a more pronounced stable boundary layer may lead to a stronger local katabatic flow from Brøggerdalen. The formation of a katabatic flow in an Arctic fjord is described by Vihma et al. (2011). In both frozen and unfrozen fjords, katabatic flows can occur, carrying cold air down from the glaciers at the edge of the fjord. In the cases measured by MASC-3, the fjord was not frozen; therefore, the air moving along the Brøggerdalen was colder and denser than the air in the fjord and stayed close to the ground. Out of the MASC-3 measurements, flight 7 shows this local katabatic flow most clearly. The backing in the wind direction at lower altitudes, which is a common feature in the vertical profiles measured by MASC-3 (Table 2), may have resulted from a less pronounced katabatic flow from Brøggerdalen mixing with the flow along the fjord in cases where the temperature difference between the air masses is not as pronounced. Only in cases like flight 7, in which there was a well-developed stable ABL and low synoptic wind speed, this local katabatic flow got strong enough to be visible in the vertical profile of the wind speed. The dominant east–south-east to south-east wind direction visible in the long-term measurements (Fig. 4a, c) resulted from a flow from the south-east (Fig. 9). In earlier studies, this flow was interpreted either as a katabatic flow (Beine et al. 2001; Argentini et al. 2003) or a channelled flow along the fjord (Esau & Repina 2012). In this regard, the MASC-3 measurements correspond well to the SODAR measurements from the ARTIST campaign (Beine et al. 2001). In the SODAR measurements, the east–south-east to south-east wind direction of the fjord flow is visible from the lowest measurement altitude up to 200–600 m a.s.l., depending on the measurement day (Beine et al. 2001). In the MASC-3 data, the fjord flow is visible at altitudes between 120 m and 500 m a.s.l., depending on the flight. For the two case studies presented here (flights 5 and 7), the fjord flow was measured between 200 m and 400 m a.s.l. over the entire horizontal extent of the flight (Fig. 5). However, the MASC-3 data do not provide any information on whether the flow along the fjord is a katabatic flow or a channelled flow. More large-scale measurements crossing the entire fjord would be necessary to investigate this.

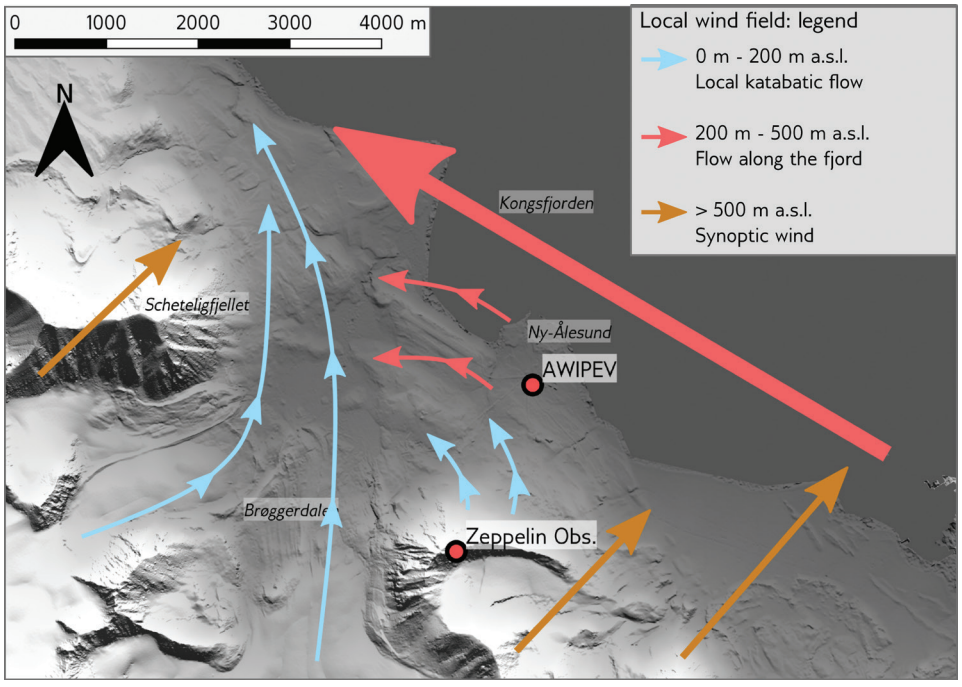

Fig. 9 Interpretation of the wind field around Ny-Ålesund, based on the measurements presented in this work. Light blue arrows show katabatic flow up to 100–200 m, and red arrows show the flow along the fjord. This flow reaches from sea level to an altitude of 500 m a.s.l. over the fjord. In Ny-Ålesund and over Brøggerdalen, it starts at 200 m a.s.l. and goes up to 500 m a.s.l. Yellow arrows show the wind above 500 m, which is already influenced by synoptic processes. The synoptic wind direction displayed represents the wind conditions on 1 May 2018 provided by AROME Arctic data (Fig. 7). Map created from Artic DEM elevation data (Porter 2018).

Citation: *Polar Research* 2022, *41*, 7884, http://dx.doi.org/10.33265/polar.v41.7884

Above the fjord flow, the wind direction turns with increasing altitude in the direction of the synoptic wind. This rotation is also visible in the long-term ground measurements and the radiosonde data (Fig. 4). At AWIPEV, and in the radiosonde measurements between 400 and 500 m a.s.l., an east–south-east wind direction dominates, rotating with increasing altitude until it matches the synoptic wind between 2000 and 2100 m a.s.l. In the case of flights 5 and 7, this rotation manifested as a veering from the fjord flow to a southern wind direction between 400 m a.s.l. and the maximum flight altitude and a further veering between the maximum flight altitude and a south-west to west–south-west wind direction at the 700 hPa level, according to the AROME data (Table 2). A backing of the wind direction with altitude is also possible if the synoptic wind has a different direction. An example of this is the SODAR wind profiles of 5 April to 7 April 1998, shown by Beine et al. (2001). Here, the fjord flow is also visible in the lower altitudes, but there is a backing of the wind direction in the upper part of the wind profiles. This is because the synoptic wind had a northern direction during the SODAR measurements (Maturilli & Kayser 2016; radiosonde data for Ny-Ålesund, 5–7 April 1998). The measurement at Zeppelinfjellet follows this rotation of the wind direction. Depending on the maximum altitude and strength of the fjord flow, the wind direction on Zeppelinfjellet deviates from the wind direction in the fjord flow. In most cases measured with MASC-3, an east–south-east to south-east wind direction at AWIPEV corresponds to a south wind direction at Zeppelinfjellet. For flight 5, the wind direction on Zeppelinfjellet corresponded to the wind direction measured above Brøggerdalen by MASC-3 (Fig. 6). However, for flight 7 and most other flights, this correspondence was not present, so other factors differentiated the wind at Zeppelin Observatory from the wind measured over Brøggerdalen. The wind direction at the Zeppelin Observatory also differed from the 925 hPa level wind direction provided by AROME during all measurement flights (Table 2). Beine et al. (2001) suggest local drainage flows along the slope of Zeppelinfjellet, which would explain the south wind directions measured at the Zeppelin Observatory (Fig. 9).

Conclusion

The measurements with MASC-3 show the flow along the Kongsfjorden, which has already been described in literature, up to altitudes above 500 m a.s.l. in several measurements. It is also shown that a local katabatic flow along Brøggerdalen has an impact on the wind field around Ny-Ålesund. Since some measurement stations around Ny-Ålesund are located within Brøggerdalen (e.g., the Gruvebadet Observatory and measurements at the Ny-Ålesund airfield), this local katabatic flow has to be considered when comparing these measurements with measurements from Ny-Ålesund village or the Zeppelin Observatory. This is important because reliable long-term data from measuring stations are essential for climate analyses. In a more direct context, the measurements made with MASC-3 in spring 2018 can be seen as a snapshot of conditions in Ny-Ålesund at that time. As climate change progresses, wind conditions in Kongsfjorden are likely to change as well. This will need to be monitored in future measurements. The MASC-3 measurements show that the wind measurements at AWIPEV in Ny-Ålesund are representative of the flow along the fjord. However, the wind measurements at the Zeppelin Observatory do not correlate to the MASC-3 measurements, the AWIPEV measurements or the synoptic wind conditions provided by the AROME model. It also becomes evident that the wind speed and direction provided by the weather prediction model data are insufficient to make a statement about the wind conditions in Ny-Ålesund. Still, the thermal stratification shown in the models can help with the interpretation of the local wind field. The MASC-3 measurements presented in this work only covered a relatively small part of Kongsfjorden, both vertically and horizontally.

Measurements on a larger scale, going across the fjord and well above the ABL, could help improve our understanding of the interaction between the Kongsfjorden wind situation and the synoptic conditions. Further measurements in the Kongsfjorden, especially during stable ABL conditions, could also provide information on the development of low-level jets, both close to Ny-Ålesund along Brøggerdalen and along Kongsfjorden. As in this work, the interaction of time-limited UAS measurements covering a dedicated area and localized but time-unlimited ground measurements have the potential to provide an accurate, comprehensive picture of a local wind field, not only in Ny-Ålesund but also in other locations with small-scale and variable wind fields influenced by a complex topography.

Acknowledgements

The authors thank the following people for their support for this work: the pilots of MASC-3, Alexander Rautenberg and Markus Schygulla; colleagues in the Environmental Physics Workgroup of the University of Tübingen, Claudio Crazzolara, Patrick Manz, Hasan Mashni and Moritz Mauz, who operated MASC-3 or provided the logistics for the measurement campaign; the team around the UAS ALADINA from the Technische Universität Braunschweig and the TROPOS Institute Leipzig, Konrad Baerfuss, Lutz Bretschneider, Ralf Kaethner and Alexander Peuker, for

all their help and support during the project; Carl Fortelius, for assisting with numerical weather prediction model analyses; Wenche Aas (NILU) and Marion Maturilli (Alfred Wegener Institute) for providing the ground and radiosonde measurements used in this work; and Andy Clifton for creating the script for the wind rose plots. Finally, the authors also thank the station leaders of AWIPEV, Piotr Kupiszewski and Rudolf Denkmann, for their support during the measurements.

Disclosure statement

The authors report no conflict of interest.

Funding

This research was funded by the German Research Foundation under the project number BA 1988/14-3.

References

Aas W. 2007a. Zeppelin Mountain meteorological measurement (wind speed). Data set. Norwegian Institute for Air Research. Accessed on the internet at https://ebas-data.nilu.no/DataSets.aspx?stations=NO0042G&nations=NO578NOR&components=wind_speed&matrices=met&fromDate=1970-01-01&toDate=2022-12-31 on 25 September 2019.

Aas W. 2007b. Zeppelin Mountain meteorological measurement (wind direction). Data set. Norwegian Institute for Air Research. Accessed on the internet at https://ebas-data.nilu.no/DataSets.aspx?stations=NO0042G&naNO578NOR&components=wind_speed&matrimet&fromDate=1970-01-01&toDate=2022-12-31 on 25 September 2019.

Altstädter B., Platis A., Wehner B., Scholtz A., Wildmann N., Hermann M., Käthner R., Baars H., Bange J. & Lampert A. 2015. ALADINA—an unmanned research aircraft for observing vertical and horizontal distributions of ultrafine particles within the atmospheric boundary layer. *Atmospheric Measurement Techniques 8*, 1627–1639, doi: 10.5194/amt-8-1627-2015.

Argentini S., Viola A.P., Mastrantonio G., Maurizi A., Georgiadis T. & Nardino M. 2003. Characteristics of the boundary layer at Ny-Ålesund in the Arctic during the ARTIST field experiment. *Annals of Geophysics 46*, 185–196, doi: 10.4401/ag-3414.

Beine H.J., Argentini S., Maurizi A., Viola A. & Mastrantonio G. 2001. The local wind field at Ny-Ålesund and the Zeppelin Mountain at Svalbard. *Meteorology and Atmospheric Physics 78*, 107–113, doi: 10.1007/s007030170009.

Cisek M., Makuch P. & Petelski T. 2017. Comparison of meteorological conditions in Svalbard fjords: Hornsund and Kongsfjorden. *Oceanologia 59*, 413–421, doi: 10.1016/j.oceano.2017.06.004.

Egerer U., Ehrlich A., Gottschalk M., Griesche H., Neggers R.A.J., Siebert H. & Wendisch M. 2021. Case study of a humidity layer above Arctic stratocumulus and potential turbulent coupling with the cloud top. *Atmospheric Chemistry and Physics 21*, 6347–6364, doi: 10.5194/acp-21-6347-2021.

Esau I. & Repina I. 2012. Wind climate in Kongsfjorden, Svalbard, and attribution of leading wind driving mechanisms through turbulence-resolving simulations. *Advances in Meteorology 2012*, article no. 568454, doi: 10.1155/2012/568454.

Ferrero L., Cappelletti D., Busetto M., Mazzola M., Lupi A., Lanconelli C., Becagli S., Traversi R., Caiazzo L., Giardi F., Moroni B., Crocchianti S., Fierz M., Močnik G., Sangiorgi G., Perrone M.G., Maturilli M., Vitale V., Udisti R. & Bolzacchini E. 2016. Vertical profiles of aerosol and black carbon in the Arctic: a seasonal phenomenology along two years (2011–2012) of field campaign. *Atmospheric Chemistry and Physics 16*, 12601–12629, doi: 10.5194/acp-16-12601-2016.

Garratt J.R. 1992. *The atmospheric boundary layer*. Cambridge: Cambridge University Press.

Hartmann J., Albers F. & Argentini S. 1999. *Arctic radiation and turbulence interaction study (ARTIST). Berichte zur Polarforschung (Reports on Polar Research) 305*. Bremerhaven: Alfred Wegener Institute for Polar and Marine Research.

Køltzow M., Casati B., Bazile E., Haiden T. & Valkonen T. 2019. An NWP model intercomparison of surface weather parameters in the European Arctic during the year of polar prediction special observing period Northern Hemisphere 1. *Weather and Forecasting 34*, 959–983, doi: 10.1175/WAF-D-19-0003.1.

Lampert A., Altstädter B., Bärfuss K., Bretschneider L., Sandgaard J., Michaelis J., Lobitz L., Asmussen M., Damm E., Käthner R., Krüger T., Lüpkes C., Nowak S., Peuker A., Rausch R., Reisder F., Scholtz A., Zakharov D.S., Gaus D., Bansmer S., Wehner B. & Pätzold F. 2020. Unmanned aerial systems for investigating the polar atmospheric boundary layer—technical challenges and examples of applications. *Atmosphere 11*, article no. 416, doi: 10.3390/atmos11040416.

Maturilli M. 2020a. Continuous meteorological observations at station Ny-Ålesund (2020-04). Data set. Alfred Wegener Institute, Research Unit Potsdam, PANGAEA®—Data Publisher for Earth & Environmental Science, doi: 10.1594/PANGAEA.925612.

Maturilli M. 2020b. Continuous meteorological observations at station Ny-Ålesund (2020-05). Data set. Alfred Wegener Institute, Research Unit Potsdam, PANGAEA®—Data Publisher for Earth & Environmental Science, doi: 10.1594/PANGAEA.925613.

Maturilli M. 2020c. High resolution radiosonde measurements from station Ny-Ålesund (2017-04 et seq). Data set. Alfred Wegener Institute, Research Unit Potsdam, PANGAEA®—Data Publisher for Earth & Environmental Science, doi: 10.1594/PANGAEA.914973.

Maturilli M. & Kayser M. 2016. Homogenized radiosonde record at station Ny-Ålesund, Spitsbergen, 1993–2014. Data set. Alfred Wegener Institute, Research Unit Potsdam,

PANGAEA®—Data Publisher for Earth & Environmental Science, doi: 10.1594/PANGAEA.845373.

MET Norway 2021. MET AROME Arctic. Data set. Accessed on the internet https://thredds.met.no/thredds/metno.html on 6 August 2021.

Müller M., Batrak Y., Kristiansen J., Køltzow M.A., Noer G. & Korosov A. 2017. Characteristics of a convective-scale weather forecasting system for the European Arctic. *Monthly Weather Review 145*, 4771–4787, doi: 10.1175/MWR-D-17-0194.1.

Petäjä T., Duplissy E.-M., Tabakova K., Schmale J., Altstädter B., Ancellet G., Arshinov M., Balin Y., Baltensperger U., Bange J., Beamish A., Belan B., Berchet A., Bossi R., Cairns W.R.L., Ebinghaus R., El Haddad I., Ferreira-Araujo B., Franck A., Huang L., Hyvärinen A., Humbert A., Kalogridis A.-C., Konstantinov P., Lampert A., MacLeod M., Magand O., Mahura A., Marelle L., Masloboev V., Moisseev D., Moschos V., Neckel N., Onishi T., Osterwalder S., Ovaska A., Paasonen P., Panchenko M., Pankratov F., Pernov J.B., Platis A., Popovicheva O., Raut J.-C., Riandet A., Sachs T., Salvatori R., Salzano R., Schröder L., Schön M., Shevchenko V., Skov H., Sonke J.E., Spolaor A., Stathopoulos V.K., Strahlendorff M., Thomas J.L., Vitale V., Vratolis S., Barbante C., Chabrillat S., Dommergue A., Eleftheriadis K., Heilimo J., Law K.S., Massling A., Noe S.M., Paris J.-D., Prévôt A.S.H., Riipinen I., Wehner B., Xie Z. & Lappalainen H.K. 2020. Overview: integrative and comprehensive understanding on polar environments (iCUPE)—concept and initial results. *Atmospheric Chemistry and Physics 20*, 8551–8592, doi: 10.5194/acp-20-8551-2020.

Porter C. 2018. Arctic DEM. Data set. University of Minnesota, doi: 10.7910/DVN/OHHUKH.

Rautenberg A., Schön M., zum Berge K., Mauz M., Manz P., Platis A., van Kesteren B., Suomi I., Kral S.T. & Bange J. 2019. The multi-purpose airborne sensor carrier MASC-3 for wind and turbulence measurements in the atmospheric boundary layer. *Sensors 19*, article no. 2292, doi: 10.3390/s19102292.

Schön M., zum Berge K., Platis A. & Bange J. 2022. UAS-based measurement of wind vector, temperature and humidity in Ny-Alesund, Svalbard, during April and May 2018. Data set. Tübingen University, PANGAEA, doi: 10.1594/PANGAEA.946961.

Svendsen H., Beszczynska-møller A., Hagen J.O., Lefauconnier B., Tverberg V., Gerland S., Ørbæk J.B., Bischof K., Papucci C., Zajaczkowski M., Azzolini R., Bruland O., Wiencke C., Winther J. & Dallmann W. 2002. The physical environment of Kongsfjorden–Krossfjorden, an Arctic fjord system in Svalbard. *Polar Research 21*, 133–166, doi: 10.3402/polar.v21i1.6479.

Tjernström M. & Graversen R.G. 2009. The vertical structure of the lower Arctic troposphere analysed from observations and the ERA-40 reanalysis. *Quarterly Journal of the Royal Meteorological Society 135*, 431–443, doi: 10.1002/qj.380.

van den Kroonenberg A., Martin T., Buschmann M., Bange J. & Vörsmann P. 2008. Measuring the wind vector using the autonomous mini aerial vehicle M2AV. *Journal of Atmospheric and Oceanic Technology 25*, 1969–1982, doi: 10.1175/2008JTECHA1114.1.

Vihma T., Kilpeläinen T., Manninen M., Sjöblom A., Jakobson E., Palo T., Jaagus J. & Maturilli M. 2011. Characteristics of temperature and humidity inversions and low-level jets over Svalbard fjords in spring. *Advances in Meteorology 2011*, article no. 486807, doi: 10.1155/2011/486807.

Wildmann N., Hofsäß M., Weimer F., Joos A. & Bange J. 2014. MASC-a small remotely piloted aircraft (RPA) for wind energy research. *Advances in Science and Research 11*, article no. 55, doi: 10.5194/asr-11-55-2014.

Wildmann N., Mauz M. & Bange J. 2013. Two fast temperature sensors for probing of the atmospheric boundary layer using small remotely piloted aircraft (RPA). *Atmospheric Measurement Techniques 6*, 2101–2113, doi: 10.5194/amt-6-2101-2013.

Wildmann N., Ravi S. & Bange J. 2014. Towards higher accuracy and better frequency response with standard multi-hole probes in turbulence measurement with remotely piloted aircraft (RPA). *Atmospheric Measurement Techniques 7*, 1027–1041, doi: 10.5194/amt-7-1027-2014.